

The Non Parametric Reconstruction of Binary Black Hole Mass Evolution from GWTC-4.0 Gravitational Wave Catalog

SAMSUZZAMAN AFROZ ¹ AND SUVODIP MUKHERJEE ¹

¹*Department of Astronomy and Astrophysics, Tata Institute of Fundamental Research, Mumbai 400005, India*

ABSTRACT

The distribution of binary black hole (BBH) masses and its evolution with redshift provide key insights into the different formation channels of compact objects and their dependence on cosmic time and stellar properties such as metallicity and star formation history. We present a non-parametric framework of the redshift evolution of the BBH mass distribution using the gravitational-wave (GW) catalogs GWTC-3 and GWTC-4 of LIGO-Virgo-KAGRA (LVK). This method simultaneously searches for the signature of any linear and quadratic redshift evolution with respect to the low-redshift population in a Bayesian framework, taking into account the detector selection effects. We find tentative evidence for a linear redshift-dependent evolution of the mass distribution, consistent over a mass range ($m \gtrsim 50 M_{\odot}$), while lower-mass systems show no significant evolution. The quadratic term remains consistent with zero, indicating that a simple linear dependence adequately describes the population up to redshift $z \sim 1$. With more GW sources in the future, this technique can reveal subtle evolutionary features in BBH populations and provide new insights into the cosmic history of black hole formation.

1. INTRODUCTION

The detection of gravitational waves (GWs) has revolutionized astrophysics by providing a direct means to observe and characterize binary black hole populations across vast cosmic distances. These unprecedented observations have transformed our understanding of how stellar mass black holes form, evolve, and merge over the history of the universe (Abbott et al. 2019, 2016; Bouffanais et al. 2021; Franciolini et al. 2022; Cheng et al. 2023; Antonelli et al. 2023; Wong et al. 2023; Tiwari & Fairhurst 2021; Tiwari 2022, 2025; Kimball et al. 2020, 2021; Afroz & Mukherjee 2025a,b,c). With each new detection, we gain invaluable information about the masses, spins, and rates of these elusive objects, enabling tests of astrophysical theory in regimes previously inaccessible (Abbott et al. 2021, 2023; LIGO-VIRGO-KAGRA Collaboration 2025a).

A fundamental question arising from these advances is whether the underlying distribution of binary black hole (BBH) masses, called as the BBH mass function changes over cosmic time. Investigating this evolution is crucial because it encodes rich information about the life cycles

of massive stars, the influence of their environments, and the physical processes shaping their end states (Mukherjee 2022; Bailes et al. 2021; Arimoto et al. 2021; Mapelli 2021; Karathanasis et al. 2023; Iorio et al. 2022; Rinaldi et al. 2025; Barrett et al. 2018; Dominik et al. 2012; Bailyn et al. 1998; Ye & Fishbach 2024; Schiebelbein-Zwack & Fishbach 2024; Rinaldi et al. 2024; Gennari et al. 2025; Lalleman et al. 2025; Sicilia et al. 2022).

Factors such as the chemical composition of progenitor stars, commonly referred to as metallicity, vary significantly across epochs and profoundly impact stellar winds and mass loss rates. Lower metallicities prevalent in the early universe likely allowed stars to retain more mass, potentially leading to the formation of heavier black holes (Karathanasis et al. 2023; Farrell et al. 2021; Belczynski et al. 2019; Spera & Mapelli 2017; Farmer et al. 2020; Hendriks et al. 2023; Farmer et al. 2019; Leung et al. 2019; Tong et al. 2025; Antonini et al. 2025b; Costa et al. 2022; Fishbach & Holz 2017; Talbot & Thrane 2018). Moreover, the universe's first generation of stars, the Population III stars, constituted metal free environments that could have produced exceptionally massive black holes distinct from those observed today (Santoliquido et al. 2023; Costa et al. 2023; Giacobbo et al. 2018; Dvorkin et al. 2016).

Understanding how these astrophysical processes imprint themselves on the black hole mass function as a

samsuzzaman.afroz@tifr.res.in

suvodip@tifr.res.in

function of redshift holds the promise of uncovering the origins and evolution of compact object populations, offering insights into star formation history, galaxy evolution, and the end stages of stellar lives. Previous studies have explored various approaches to characterize the BBH mass distribution and its potential evolution, ranging from parametric models with specific functional forms to more flexible non-parametric methods (Wysocki et al. 2019; Mandel et al. 2019; Tiwari & Fairhurst 2021; Talbot et al. 2019; Wong et al. 2020; Callister & Farr 2024; Riley & Mandel 2023; Farah et al. 2025; Talbot et al. 2025; Ray et al. 2023; Magaña Hernandez & Palmese 2025; Antonini et al. 2025a; Edelman et al. 2023; Heinzel et al. 2025b, 2023, 2025a; Alvarez-Lopez et al. 2025).

The two major open questions regarding the redshift evolution of the BBH mass distribution are: (i) Does a single, global BBH mass distribution adequately describe the population across all redshifts, or is such a description valid only within restricted redshift ranges? (ii) If not, does the BBH mass distribution itself evolve with redshift, and if so, what is the nature of that evolution? The challenge in answering these questions lies with our ignorance in modelling either of these from first principle due to large astrophysical uncertainties. Along with the theoretical uncertainties, selection effects also plays a major role.

In order to infer the true physical effect from the data, one needs to take into account the redshift and mass dependent selection effects. Gravitational wave detectors have sensitivity biases favoring the detection of more massive and nearby sources, creating a mass and redshift dependent selection function effect, which can be modeled given the detectors sensitivity (Essick 2023; Essick & Holz 2024; Messenger & Veitch 2013; Gerosa & Bellotti 2024; Essick et al. 2025).

In this work, we propose a fully non parametric framework for inferring the evolution of the stellar mass black hole mass function using GW observations. Leveraging a Taylor series expansion of the joint mass redshift distribution, this approach makes minimal assumptions about the functional form of the mass function or its evolution. Instead, it allows the data itself to reveal evolutionary patterns, capturing both linear and higher order changes in the population over redshift. This strategy offers greater flexibility and interpretability, with each Taylor coefficient corresponding to physically meaningful rates and accelerations of population change. Such a framework paves the way for revealing subtle and complex evolutionary signatures that could otherwise remain hidden. Applying this framework to the GWTC-3 (Abbott et al. 2023) and GWTC-4 catalog (LIGO-VIRGO-

KAGRA Collaboration 2025b), the most comprehensive collection of BBH mergers to date, we find tentative evidence for mass dependent evolution in the BBH mass function. High mass systems (40-60 M_{\odot}) very mild indications of positive redshift evolution, while lighter black holes exhibit little or no statistically significant evolution.

These results are consistent with metallicity driven formation channels and demonstrate the potential of non-parametric methods for probing black hole populations with future GW observations.

2. NON-PARAMETRIC BAYESIAN INFERENCE OF THE BBH MASS DISTRIBUTION WITH REDSHIFT

The aim of this work is to test whether the distribution of BBH component masses evolves with redshift, a question with direct implications for stellar evolution, metallicity, and the astrophysical environments of BBH formation. Gravitational wave observations provide unique access to this distribution, but detector sensitivity introduces strong selection effects: massive systems are detectable at greater distances than lighter ones, biasing the observed sample. Correcting for these biases is essential for reconstructing the intrinsic population. We demonstrate in this section our Bayesian framework for the reconstruction of the BBH mass distribution from data using a flexible, non-parametric approach.

2.1. Non-Parametric Mass-Redshift Distribution

Rather than relying on parametric models with fixed functional forms, which risk obscuring unanticipated features, we adopt a non-parametric framework based on a Taylor expansion of the mass-redshift distribution. Instead of prescribing exact shapes, this method expresses $p(m, z)$ as a smooth series expansion in redshift around a reference redshift z_{ref} :

$$p(m, z) = \sum_{n=0}^N \frac{1}{n!} \left. \frac{\partial^n p(m, z)}{\partial z^n} \right|_{z=z_{\text{ref}}} (z - z_{\text{ref}})^n, \quad (1)$$

where the truncation order N dictates the level of evolutionary behavior captured, and we choose $z_{\text{ref}} = 0.25$ to center the expansion. In this work, we restrict our analysis to the second-order term in the Taylor series expansion, justified by the fact that the redshift range of current GW observations extends up to $z \sim 1.0$, with only a few detected events at high redshift. The resulting approximation is:

$$p(m, z) \approx p_0(m) + p_1(m)(z - z_{\text{ref}}) + p_2(m)(z - z_{\text{ref}})^2, \quad (2)$$

with the coefficient functions defined as:

$$\begin{aligned} p_0(m) &\equiv p(m, z_{\text{ref}}), & p_1(m) &\equiv \left. \frac{\partial p}{\partial z} \right|_{z_{\text{ref}}}, \\ p_2(m) &\equiv \left. \frac{1}{2} \frac{\partial^2 p}{\partial z^2} \right|_{z_{\text{ref}}}. \end{aligned} \quad (3)$$

Here, $p_0(m)$ encodes the mass distribution at the reference redshift, while $p_1(m)$ and $p_2(m)$ capture the linear and quadratic evolutionary trends, respectively. This construction avoids restrictive parametric assumptions, permits non-monotonic evolution, and provides coefficients with direct physical interpretations.

Since the Taylor expansion does not automatically satisfy probability normalization, in our analysis we explicitly normalize the resulting expression at each redshift by dividing by its integral over mass. This ensures that $\int p(m | z, \theta) dm = 1$ at each redshift, making $p(m | z, \theta)$ a valid conditional probability distribution for mass given redshift. The recovered evolution coefficients encode distinct aspects of mass function evolution. The linear evolution coefficient $p_1(m)$ indicates whether black holes of mass m were more common (positive values) or less common (negative values) at higher redshifts. The magnitude $|p_1(m)|$ quantifies the strength of evolution. The quadratic evolution coefficient $p_2(m)$ captures curvature in evolutionary trends. Positive values of $p_2(m)$ indicate accelerating evolution, while negative values suggest deceleration. This term allows for non-monotonic behavior and can reveal whether evolutionary processes are intensifying or saturating with redshift.

2.2. Data Processing and Selection Function

We analyze BBH mergers from the GWTC-3 (Abbott et al. 2023) and GWTC-4 (LIGO-VIRGO-KAGRA Collaboration 2025b) catalogs, using publicly released posterior samples from the LVK parameter estimation analyses. For each detected event i and posterior sample s , we obtain source-frame component masses ($m_{1,s}^{(i)}, m_{2,s}^{(i)}$) and a luminosity distance sample $d_{L,s}^{(i)}$. Adopting a spatially flat Λ CDM cosmology with parameters from PLANCK 2018 (Aghanim et al. 2020), the luminosity distance as a function of redshift is:

$$d_L(z) = (1+z) \frac{c}{H_0} \int_0^z \frac{dz'}{\sqrt{\Omega_m(1+z')^3 + (1-\Omega_m)}}, \quad (4)$$

where Ω_m is the matter density and H_0 is the Hubble constant. We convert each distance sample $d_{L,s}^{(i)}$ to a redshift $z_s^{(i)}$ using this relation, mapping the posteriors into the (m, z) plane. We work consistently in the source frame for easier interpretation of any redshift evolution signatures.

To compute the selection function, we use the publicly released LVK injection campaigns associated with GWTC-3 and GWTC-4¹. These injection campaigns provide simulated compact binary coalescence signals spanning the relevant parameter space. We classify an injection as detected if its network signal-to-noise ratio satisfies $\text{SNR} > 10$. We note that while GWTC detections are defined using a false alarm rate (FAR) threshold, we adopt the SNR cut for the injection sets as this threshold is commonly used in population inference studies and provides a conservative approximation to the FAR-based selection criterion for the bulk of the BBH population. This choice is consistent with previous population analyses and ensures computational tractability while capturing the essential sensitivity characteristics of the detector network.

The selection function $S(m, z)$ represents the probability that a binary with component mass m at redshift z is detected by the GW network. Formally, this corresponds to marginalizing the detection probability over extrinsic parameters Ω (e.g., sky location, inclination, and polarization):

$$S(m, z) = \int P(\text{det} | m, z, \Omega) p(\Omega) d\Omega \approx \frac{N_{\text{det}}(m, z)}{N_{\text{inj}}(m, z)}, \quad (5)$$

where the integral is estimated empirically using the injection campaigns described above. In practice, $S(m, z)$ is computed as the fraction of injected signals that are recovered in each region of the (m, z) plane. To avoid numerical instabilities in sparsely populated regions of the injection parameter space, we impose a small floor on the selection function and require $S(m, z) \geq 10^{-3}$.

Because the injection sets span realistic distributions of mass ratios, spins, and orientations, the resulting selection function automatically incorporates spin- and geometry-dependent detection efficiencies. By working directly with the component mass posteriors (m_1, m_2), we effectively marginalize over these secondary parameters without imposing restrictive parametric assumptions about their redshift evolution.

2.3. Hierarchical Inference Framework

We develop a hierarchical Bayesian framework that properly accounts for measurement uncertainties in individual event parameters and detector selection effects. Our approach builds on the standard hierarchical inference methodology established in gravitational wave pop-

¹ The injection sets and recovered selection functions for GWTC-3 and GWTC-4 are publicly available at <https://zenodo.org/record/5636816> and <https://zenodo.org/records/16740128>, respectively.

ulation studies (Mandel et al. 2019; Fishbach et al. 2017; Loredo 2004), adapted to our non-parametric, binned representation of the mass-redshift distribution. We discretize the continuous (m, z) parameter space into a two-dimensional grid of bins $\{(m_k, z_j)\}$ with $k = 1, \dots, N_m$ mass bins and $j = 1, \dots, N_z$ redshift bins.

This bin approach minimizes assumptions about smoothness or correlations between neighboring regions, allowing the data to reveal localized evolutionary features without imposing artificial constraints. The intrinsic number of mergers in bin (m_k, z_j) is:

$$N_{\text{int}}(m_k, z_j | \theta_{kj}) = T_{\text{obs}} \mathcal{R}(z_j) p(m_k | z_j, \theta_{kj}) \times \left. \frac{dV_c}{dz} \right|_{z_j} \frac{1}{1+z_j} \Delta m_k \Delta z_j, \quad (6)$$

where T_{obs} is the observation time, $\mathcal{R}(z_j)$ is the merger rate density, dV_c/dz is the differential comoving volume, and $(1+z)^{-1}$ accounts for time dilation. This represents mergers that *actually occur* in the universe, independent of detection. The expected number of detections is $N_{\text{exp}}(m_k, z_j | \theta_{kj}) = N_{\text{int}}(m_k, z_j | \theta_{kj}) \times S(m_k, z_j)$, where the selection function $S(m_k, z_j)$ accounts for detector sensitivity.

For each event i and bin (k, j) , we compute the posterior weight:

$$W_{ijk} = \frac{1}{N_s} \sum_{\substack{\text{samples } \ell \\ \text{in bin } (k,j)}} \frac{1}{\pi(m_{i,\ell}, z_{i,\ell})}, \quad (7)$$

where $\{m_{i,\ell}, z_{i,\ell}\}_{\ell=1}^{N_s}$ are the posterior samples for event i , and $\pi(m, z)$ is the parameter estimation prior. This weight represents the fractional posterior support that event i has in bin (k, j) , events.

The hierarchical likelihood for bin (k, j) with parameters θ_{kj} is:

$$\mathcal{L}(\theta_{kj}) = e^{-N_{\text{exp}}(m_k, z_j | \theta_{kj})} \prod_{i=1}^{N_{\text{obs}}} \left[W_{ijk} \frac{N_{\text{int}}(m_k, z_j | \theta_{kj})}{\Delta m_k \Delta z_j} \right], \quad (8)$$

here, the product is over the observed events.

3. OBSERVED BBH POPULATION AND EVIDENCE FOR MASS DISTANCE TRENDS

We analyze BBH mergers from the GWTC-3 (Abbott et al. 2023) and GWTC-4 (LIGO-VIRGO-KAGRA Collaboration 2025b) catalog, the most comprehensive public collection of GW detections to date. For each catalog event we draw posterior samples of the source frame component masses, (m_1, m_2) , and luminosity distance, d_L . Distances are converted to

redshift assuming a spatially flat Λ CDM cosmology with PLANCK 2018 parameters ($H_0 = 67.4 \text{ km s}^{-1} \text{ Mpc}^{-1}$, $\Omega_m = 0.315$) (Aghanim et al. 2020), which maps every posterior sample into the (m, z) plane.

Figure 1 presents the resulting mass-redshift distributions of primary mass (left) and secondary mass (right) constructed from these posterior samples across all 176 events. Each 2D histogram uses prior reweighting to recover the intrinsic population-level distribution, revealing the characteristic BBH mass hierarchy and redshift evolution over $m \in [5, 100] M_\odot$, $z \in [0, 1.2]$.

The observed distribution of the GW sources in the mass and redshift plane can arise from two non exclusive effects. First, heavier binaries generate stronger GW signals and are therefore detectable at larger distances; this selection bias alone can produce an apparent mass redshift correlation even if the intrinsic population is non evolving. Second, there may be genuine astrophysical evolution of the BBH mass function for example, metallicity driven differences in stellar winds and mass loss, that enhances the formation of massive remnants at earlier cosmic times. Disentangling these two effects requires quantitative correction for detector sensitivity and measurement uncertainty.

To distinguish between genuine evolution of the BBH mass distribution and observational biases, we employ the LVK injection campaigns Observing Runs O1-O4. The selection function, together with the full posterior samples of the observed events, is incorporated into our hierarchical Bayesian framework (Section 2). This framework models the intrinsic joint distribution $p(m, z)$ via Taylor expansion, while explicitly marginalizing over measurement uncertainties and correcting for selection effects. The results of this analysis are presented in Section 4.

4. RESULTS

We apply the non parametric Bayesian framework described in Section 2 to the GWTC-3 and GWTC-4 catalog of BBH mergers, incorporating the corresponding injection campaigns to account for detector selection effects. The analysis is performed in the (m, z) plane, discretized into grids of varying resolutions to study the impact of bin size on the results. We consider two cases: one with $\Delta m = 10 M_\odot$ and $\Delta z = 0.1$, and another with a finer grid having $\Delta m = 5 M_\odot$ and $\Delta z = 0.1$. Both cases cover the redshift range $0 \leq z \leq 1$ and mass range $10 M_\odot \leq m \leq 80 M_\odot$. The detector selection function $S(m, z)$ is calibrated from the injection campaign of LVK collaboration.

The Bayesian inference was performed using the `emcee` (Foreman-Mackey et al. 2013) affine-invariant en-

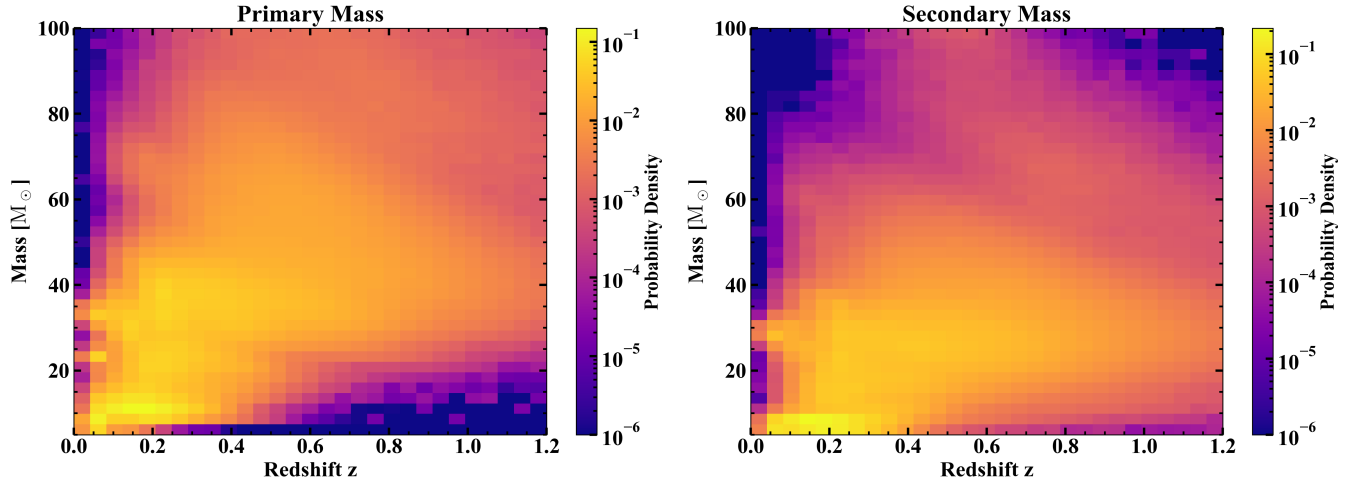


Figure 1. Mass-redshift distributions for the primary (left) and secondary (right) black hole components in GWTC-4 catalog. Each distribution combines individual-event posterior samples with prior weighting.

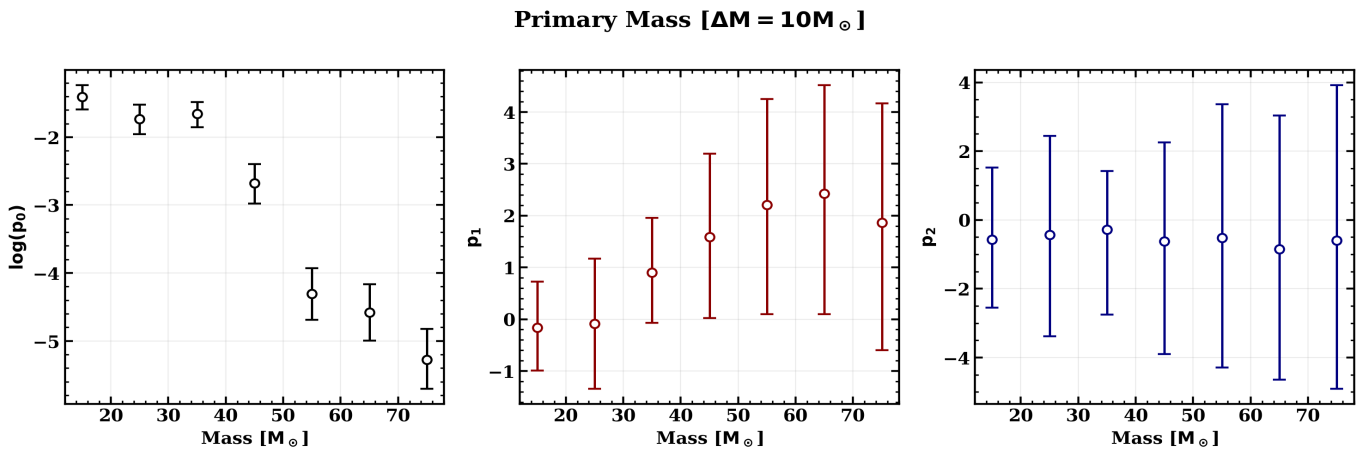


Figure 2. Posterior constraints on the redshift evolution of the BBH primary mass (m_1) distribution for a binning scheme with $\Delta M = 10 M_\odot$ and $\Delta z = 0.1$. **Left:** Constant coefficient $\log(P_0)$ describing the baseline primary mass distribution. **Middle:** Linear coefficient P_1 , quantifying the first-order variation of the mass distribution with redshift. **Right:** Quadratic coefficient P_2 , probing possible curvature in the redshift dependence. Error bars represent 1σ credible intervals obtained from the hierarchical Bayesian analysis. The linear coefficient is consistent with zero at low masses ($m_1 \lesssim 30 M_\odot$) and shows a mild positive trend toward higher masses, suggesting that more massive black holes may be relatively more abundant at earlier cosmic times. The quadratic coefficient remains consistent with zero across all mass bins, indicating that a linear redshift dependence adequately describes the population within the current observational range $z \lesssim 1$ accessible to LVK.

semble Markov Chain Monte Carlo (MCMC) sampler. For the finer mass binning configuration ($\Delta M = 5 M_\odot$), we used 200 walkers and ran the chains for 50 000 steps, discarding the first 10 000 steps as burn-in. For the coarser binning configuration ($\Delta M = 10 M_\odot$), we used 100 walkers with 25 000 steps and removed the first 5 000 steps as burn-in. Uniform priors were adopted for all Taylor expansion coefficients describing the mass evolution, with $\log P_0 \in [-13, 0]$, $P_1 \in [-20, 20]$, and $P_2 \in [-30, 30]$.

Figures 2-5 summarize the key results of our non-parametric reconstruction of the redshift evolution of

the BBH mass distribution. We present constraints separately for the primary mass (m_1) and secondary mass (m_2). For the primary mass (m_1), a clear qualitative trend emerges in the linear coefficient $p_1(m_1)$. In both binning schemes, $p_1(m_1)$ is consistent with zero at low masses ($m_1 \lesssim 25\text{-}30 M_\odot$), indicating no statistically significant redshift evolution in this regime. Toward higher masses, however, $p_1(m_1)$ shifts systematically toward positive values. In the large-bin case, this manifests as a smooth rise of the linear coefficient beyond $\sim 40 M_\odot$, while in the finer binning the trend becomes more structured but remains qualitatively similar. This behavior

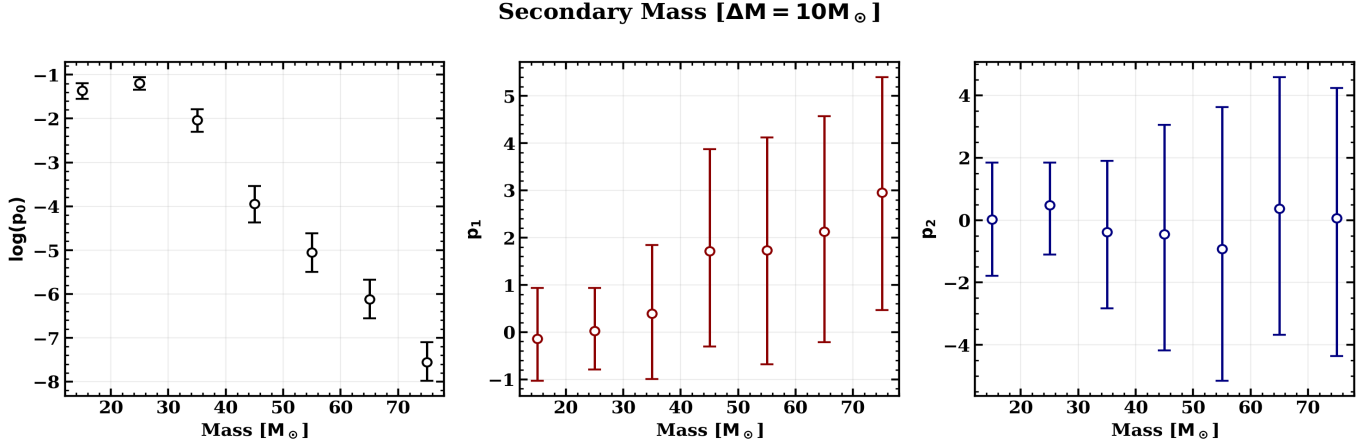


Figure 3. Posterior constraints on the redshift evolution of the BBH secondary mass (m_2) distribution for a binning scheme with $\Delta M = 10 M_{\odot}$ and $\Delta z = 0.1$. **Left:** Constant coefficient $\log(P_0)$ describing the baseline primary mass distribution. **Middle:** Linear coefficient P_1 , quantifying the first-order variation of the mass distribution with redshift. **Right:** Quadratic coefficient P_2 , probing possible curvature in the redshift dependence. Error bars represent 1σ credible intervals obtained from the hierarchical Bayesian analysis. The linear coefficient is consistent with zero at low masses ($m_1 \lesssim 30 M_{\odot}$) and shows a mild positive trend toward higher masses, suggesting that more massive black holes may be relatively more abundant at earlier cosmic times. The quadratic coefficient remains consistent with zero across all mass bins, indicating that a linear redshift dependence adequately describes the population within the current observational range $z \lesssim 1$ accessible to LVK.

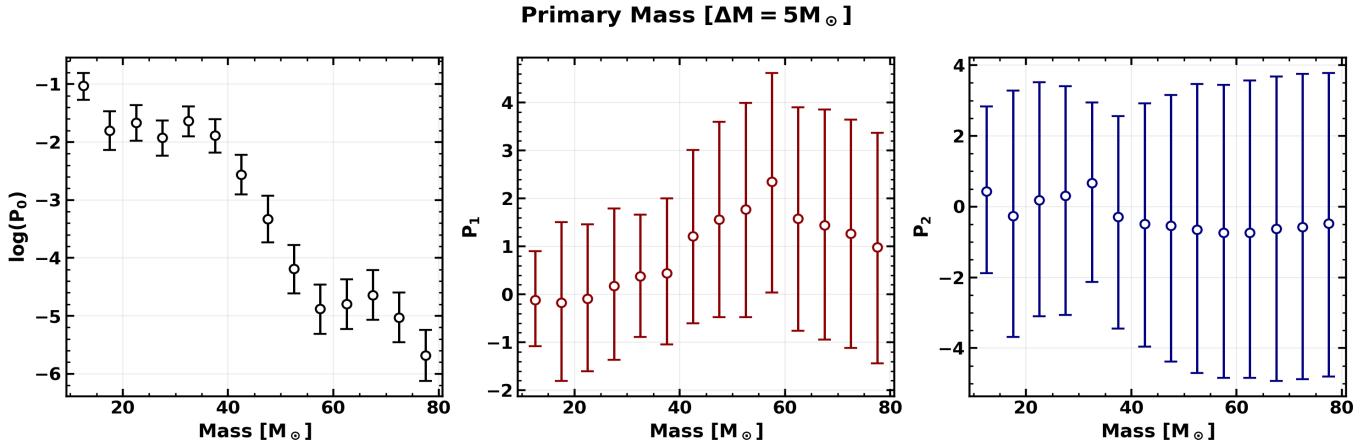


Figure 4. Posterior constraints on the redshift evolution of the BBH primary mass (m_1) distribution for a binning scheme with $\Delta M = 5 M_{\odot}$ and $\Delta z = 0.1$. **Left:** Constant coefficient $\log(P_0)$ describing the baseline primary mass distribution. **Middle:** Linear coefficient P_1 , quantifying the first-order variation of the mass distribution with redshift. **Right:** Quadratic coefficient P_2 , probing possible curvature in the redshift dependence. Error bars represent 1σ credible intervals obtained from the hierarchical Bayesian analysis. The linear coefficient is consistent with zero at low masses ($m_1 \lesssim 30 M_{\odot}$) and shows a mild positive trend toward higher masses, suggesting that more massive black holes may be relatively more abundant at earlier cosmic times. The quadratic coefficient remains consistent with zero across all mass bins, indicating that a linear redshift dependence adequately describes the population within the current observational range $z \lesssim 1$ accessible to LVK.

suggests that more massive primary black holes were relatively more abundant at earlier cosmic times, consistent with astrophysical scenarios in which lower metallicity environments at higher redshift favor the formation of heavier remnants. The full posterior distributions of the inferred parameters, including the corresponding corner plots for both binning configurations, are presented in Appendix A.

In contrast, the quadratic coefficient $p_2(m_1)$ remains statistically consistent with zero across nearly all mass bins for both discretizations. Although fluctuations are visible, particularly in the finer binning, they are well within the 1σ uncertainties. This indicates no compelling evidence for strong curvature in the redshift dependence of the primary mass distribution within the currently accessible range $z \lesssim 1$ probed by LVK.

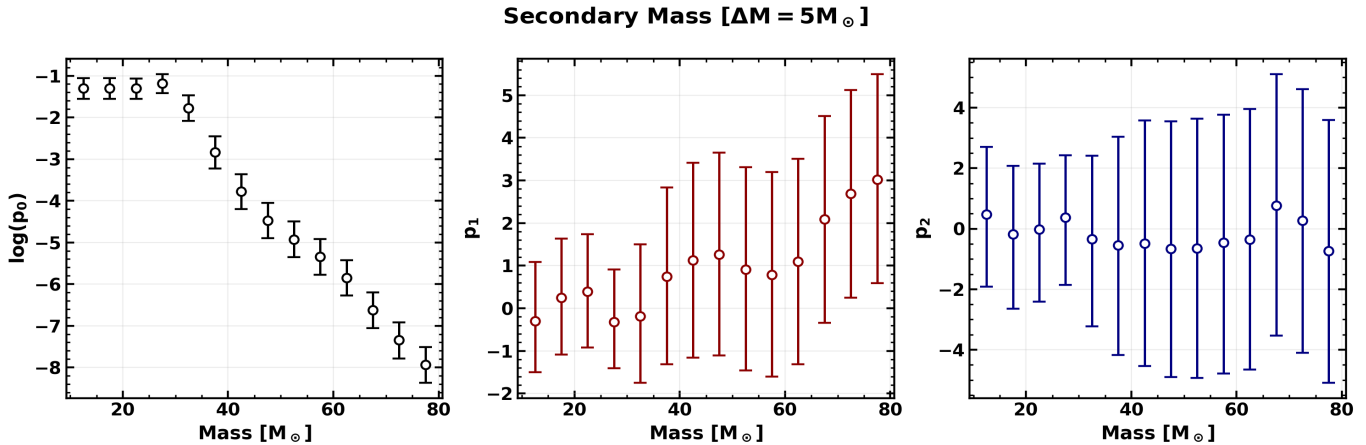


Figure 5. Posterior constraints on the redshift evolution of the BBH secondary mass (m_2) distribution for a binning scheme with $\Delta M = 5 M_\odot$ and $\Delta z = 0.1$. **Left:** Constant coefficient $\log(P_0)$ describing the baseline primary mass distribution. **Middle:** Linear coefficient P_1 , quantifying the first-order variation of the mass distribution with redshift. **Right:** Quadratic coefficient P_2 , probing possible curvature in the redshift dependence. Error bars represent 1σ credible intervals obtained from the hierarchical Bayesian analysis. The linear coefficient is consistent with zero at low masses ($m_1 \lesssim 30 M_\odot$) and shows a mild positive trend toward higher masses, suggesting that more massive black holes may be relatively more abundant at earlier cosmic times. The quadratic coefficient remains consistent with zero across all mass bins, indicating that a linear redshift dependence adequately describes the population within the current observational range $z \lesssim 1$ accessible to LVK.

A broadly similar picture emerges for the secondary mass (m_2), albeit with larger statistical uncertainties. For the coarser binning ($\Delta m = 10, M_\odot$), the linear coefficient $p_1(m_2)$ shows a gradual increase toward higher masses, with low-mass bins consistent with zero and high-mass bins favoring positive values. In the finer binning, this increasing trend persists but appears noisier, with larger error bars reflecting the reduced number of events per bin. Nevertheless, the overall pattern is consistent with that observed for the primary mass: a tendency for more massive components to exhibit stronger positive redshift evolution.

The quadratic coefficient for secondary mass $p_2(m_2)$ does not display any statistically significant deviation from zero across the mass range. While individual bins fluctuate above or below zero, the uncertainties remain large and encompass the null hypothesis of no quadratic evolution. Therefore, within current observational precision, a linear redshift dependence appears sufficient to describe the secondary mass evolution as well.

Our analysis marginalizes over mass ratio and spin distributions by working directly with component masses and using selection functions from comprehensive injection campaigns. Black hole spins remain poorly constrained in current GW observations, and we do not model their potential redshift evolution. However, the mass-dependent detector sensitivity is dominated by the chirp mass dependence of GW amplitude, with spins contributing subdominant corrections, ensuring our mass evolution inferences are robust to spin distribution uncertainties.

Our findings can be compared with previous population studies using GWTC-3. [Fishbach et al. \(2021\)](#) found hints of increasing characteristic mass with redshift using parametric models, qualitatively consistent with our mildly positive $p_1(m)$ at high masses. [Tiwari \(2022\)](#) reported results consistent with no evolution across all masses, which aligns with our findings at $m \lesssim 30 M_\odot$ but differs at higher masses where very weak indications of evolution. [Karathanasis et al. \(2023\)](#) explored metallicity-dependent evolution scenarios and found weak evidence for mass evolution, corroborating our mass-dependent trends. The inclusion of GWTC-4 data, with its extended redshift reach and increased event count, allows our non-parametric approach to reveal mass-resolved evolutionary features that may have been obscured in earlier parametric analyses or smaller catalogs.

Taken together, the figure demonstrates that the observed BBH population is consistent with a scenario in which the abundance of massive black holes increases modestly with redshift, while lower mass systems remain approximately constant. The mass dependent nature of this evolution strongly points to environmental effects such as metallicity shaping the efficiency of massive black hole formation across cosmic time.

5. CONCLUSIONS

We have developed and applied a fully non-parametric Bayesian framework to infer the redshift evolution of the BBH mass distribution using all confident BBH detections from the LVK GWTC-3 and GWTC-4 catalogs.

By expanding the intrinsic joint distribution $p(m, z)$ as a Taylor series around $z_{\text{ref}} = 0.25$, the method captures evolutionary trends without imposing restrictive parametric assumptions, while rigorously accounting for detector selection effects through injection calibrated efficiencies.

Our analysis yields very mild evidence for mass-dependent evolution. The linear evolution coefficient $p_1(m)$ is consistent with zero for lower mass systems ($m \lesssim 30 M_{\odot}$), but becomes increasingly positive at higher masses. In particular, the highest mass bins show very mild indications that massive black holes may have been relatively more abundant at earlier cosmic times. By contrast, the quadratic term $p_2(m)$ remains consistent with zero across all mass ranges, indicating that a linear description suffices up to the redshift range $z \sim 1$ currently probed by LVK observations.

These results are qualitatively consistent with theoretical expectations for metallicity driven evolution: low metallicity environments at high redshift suppress stellar winds, allowing the formation of more massive stellar cores and correspondingly heavier black hole remnants. The lack of detectable evolution for lower mass systems suggests that their formation channels are less sensitive to environmental variations, consistent with robust core collapse pathways. The approximately linear trend indicates gradual, metallicity driven changes over cosmic time rather than abrupt evolutionary transitions. This trend is qualitatively consistent with the probability of different formation channels inferred from phase-space analyses, showing that above approximately $45 M_{\odot}$ there is an indication of a different population of BBHs (Afroz & Mukherjee 2025c).

Beyond these specific findings, this work demonstrates the power of non-parametric approaches for GW population inference. Unlike parametric models, which may obscure or bias subtle features, our Taylor expansion framework provides a flexible yet interpretable means of capturing population trends while fully correcting for observational selection effects (see Section 2). The method’s ability to probe possible mass-dependent evolution highlights its value for future analyses with larger datasets.

Previous studies based on GWTC-3 (Fishbach et al. 2021; van Son et al. 2022; Tiwari 2022; Karathanasis et al. 2023; Rinaldi et al. 2024; Heinzl et al. 2025b; Lalleman et al. 2025) reported mixed evidence for mass-redshift evolution, ranging from no detectable trends to weak indications at high masses. Some works found hints of increasing characteristic mass with redshift (Fishbach et al. 2021), while others reported results consistent with no evolution (Tiwari 2022). Our com-

bined GWTC-3 and GWTC-4 analysis, employing a complementary non-parametric approach with mass resolved evolution coefficients, finds very mild evidence for evolution at high masses, while providing new insights into where (in mass) such evolution may be most pronounced.

Looking forward, the increase in detection rates expected from next generation ground based detectors such as Cosmic Explorer (Reitze et al. 2019) and the Einstein Telescope (Branchesi et al. 2023) will extend BBH catalogs to higher redshift, enabling reconstruction of higher order evolutionary features with high statistical precision. Our non parametric methodology is well positioned to exploit these datasets, offering both robustness and flexibility in probing the cosmic history of black hole formation. As GW astronomy transitions into the precision era, such model independent frameworks will be essential for extracting the full astrophysical information encoded in BBH populations, ultimately linking GW observations to stellar evolution, galactic chemical enrichment, and the early universe.

ACKNOWLEDGMENTS

The authors express their gratitude to Souradeep Pal for reviewing the manuscript and providing useful comments as a part of the LIGO publication policy. This work is part of the `<data|theory>` Universe Lab, supported by TIFR and the Department of Atomic Energy, Government of India. The authors express gratitude to the system administrator of the computer cluster of `<data|theory>` Universe Lab. This research is supported by the Prime Minister Early Career Research Award, Anusandhan National Research Foundation, Government of India. We thank the LIGO Scientific Collaboration, the Virgo Collaboration, and the KAGRA Collaboration for providing the gravitational-wave data through the Gravitational Wave Open Science Center (GWOSC). LIGO, funded by the U.S. National Science Foundation (NSF), and Virgo, supported by the French CNRS, Italian INFN, and Dutch Nikhef, along with contributions from Polish and Hungarian institutes. This collaborative effort is backed by the NSF’s LIGO Laboratory, a major facility fully funded by the National Science Foundation. The research leverages data and software from the Gravitational Wave Open Science Center, a service provided by LIGO Laboratory, the LIGO Scientific Collaboration, Virgo Collaboration, and KAGRA. Advanced LIGO’s construction and operation receive support from STFC of the UK, Max Planck Society (MPS), and the State of Niedersachsen/Germany, with additional backing from the Australian Research Council. Virgo, affiliated with the Eu-

ropean Gravitational Observatory (EGO), secures funding through contributions from various European institutions. Meanwhile, KAGRA’s construction and operation are funded by MEXT, JSPS, NRF, MSIT, AS, and MoST. This material is based upon work supported by NSF’s LIGO Laboratory which is a major facility

fully funded by the National Science Foundation. We acknowledge the use of the following packages in this work: Numpy (Van Der Walt et al. 2011), Scipy (Jones et al. 2001–), Matplotlib (Hunter 2007), Astropy (Robitaille et al. 2013), pygtdc (Bocquet & Carter 2016), and emcee (Foreman-Mackey et al. 2013).

APPENDIX

A. POSTERIOR DISTRIBUTIONS OF EVOLUTION COEFFICIENTS

In this appendix we present the full posterior distributions of the non-parametric evolution coefficients inferred in our hierarchical Bayesian analysis. The intrinsic mass-redshift distribution is expanded as a Taylor series in redshift,

$$p(m, z) = p_0(m) + p_1(m)(z - z_{\text{ref}}) + p_2(m)(z - z_{\text{ref}})^2, \quad (\text{A1})$$

where $p_0(m)$ represents the baseline mass distribution, while $p_1(m)$ and $p_2(m)$ capture the linear and quadratic redshift evolution of the population, respectively. We show the full posterior distributions and parameter correlations using corner plots. These visualizations provide a comprehensive view of parameter uncertainties, degeneracies, and the stability of the hierarchical inference across different binning choices.

Figures 6 and 7 show the posterior distributions for the primary mass coefficients using coarse ($\Delta M = 10M_{\odot}$) and fine ($\Delta M = 5M_{\odot}$) mass binning schemes, respectively. Figures 8 and 9 show the corresponding results for the secondary mass coefficients. The diagonal panels show the marginalized one-dimensional posterior distributions for each parameter, while the off-diagonal panels display the two-dimensional joint posteriors with 1σ and 2σ credible regions.

DATA AVAILABILITY

The gravitational wave catalogs used in this study are publicly available on Zenodo as part of the LVK data releases: LVK Scientific Collaboration (2021a), LVK Scientific Collaboration (2021b), and LVK Scientific Collaboration (2025).

REFERENCES

- Abbott, B. P., et al. 2016, *Phys. Rev. Lett.*, 116, 061102, doi: [10.1103/PhysRevLett.116.061102](https://doi.org/10.1103/PhysRevLett.116.061102)
- . 2019, *Phys. Rev. X*, 9, 031040, doi: [10.1103/PhysRevX.9.031040](https://doi.org/10.1103/PhysRevX.9.031040)
- Abbott, R., et al. 2021, *Astrophys. J. Lett.*, 913, L7, doi: [10.3847/2041-8213/abe949](https://doi.org/10.3847/2041-8213/abe949)
- . 2023, *Phys. Rev. X*, 13, 011048, doi: [10.1103/PhysRevX.13.011048](https://doi.org/10.1103/PhysRevX.13.011048)
- Afroz, S., & Mukherjee, S. 2025a, *Phys. Rev. D*, 112, 023531, doi: [10.1103/7zc2-g9vq](https://doi.org/10.1103/7zc2-g9vq)
- . 2025b. <https://arxiv.org/abs/2505.22739>
- . 2025c. <https://arxiv.org/abs/2509.09123>
- Aghanim, N., et al. 2020, *Astron. Astrophys.*, 641, A6, doi: [10.1051/0004-6361/201833910](https://doi.org/10.1051/0004-6361/201833910)
- Alvarez-Lopez, S., Heinzl, J., Mould, M., & Vitale, S. 2025. <https://arxiv.org/abs/2506.20731>
- Antonelli, A., Kritos, K., Ng, K. K. Y., Cotesta, R., & Berti, E. 2023, *Phys. Rev. D*, 108, 084044, doi: [10.1103/PhysRevD.108.084044](https://doi.org/10.1103/PhysRevD.108.084044)
- Antonini, F., Callister, T., Dosopoulou, F., Romero-Shaw, I., & Chattopadhyay, D. 2025a. <https://arxiv.org/abs/2506.09154>
- Antonini, F., Romero-Shaw, I., Callister, T., et al. 2025b. <https://arxiv.org/abs/2509.04637>
- Arimoto, M., et al. 2021, arXiv preprint. <https://arxiv.org/abs/2104.02445>
- Bailes, M., et al. 2021, *Nature Rev. Phys.*, 3, 344, doi: [10.1038/s42254-021-00303-8](https://doi.org/10.1038/s42254-021-00303-8)
- Bailyn, C. D., Jain, R. K., Coppi, P., & Orosz, J. A. 1998, *Astrophys. J.*, 499, 367, doi: [10.1086/305614](https://doi.org/10.1086/305614)
- Barrett, J. W., Gaebel, S. M., Neijssel, C. J., et al. 2018, *Mon. Not. Roy. Astron. Soc.*, 477, 4685, doi: [10.1093/mnras/sty908](https://doi.org/10.1093/mnras/sty908)
- Belczynski, K., Hirschi, R., Kaiser, E. A., et al. 2019, doi: [10.3847/1538-4357/ab6d77](https://doi.org/10.3847/1538-4357/ab6d77)
- Bocquet, S., & Carter, F. W. 2016, *The Journal of Open Source Software*, 1, doi: [10.21105/joss.00046](https://doi.org/10.21105/joss.00046)

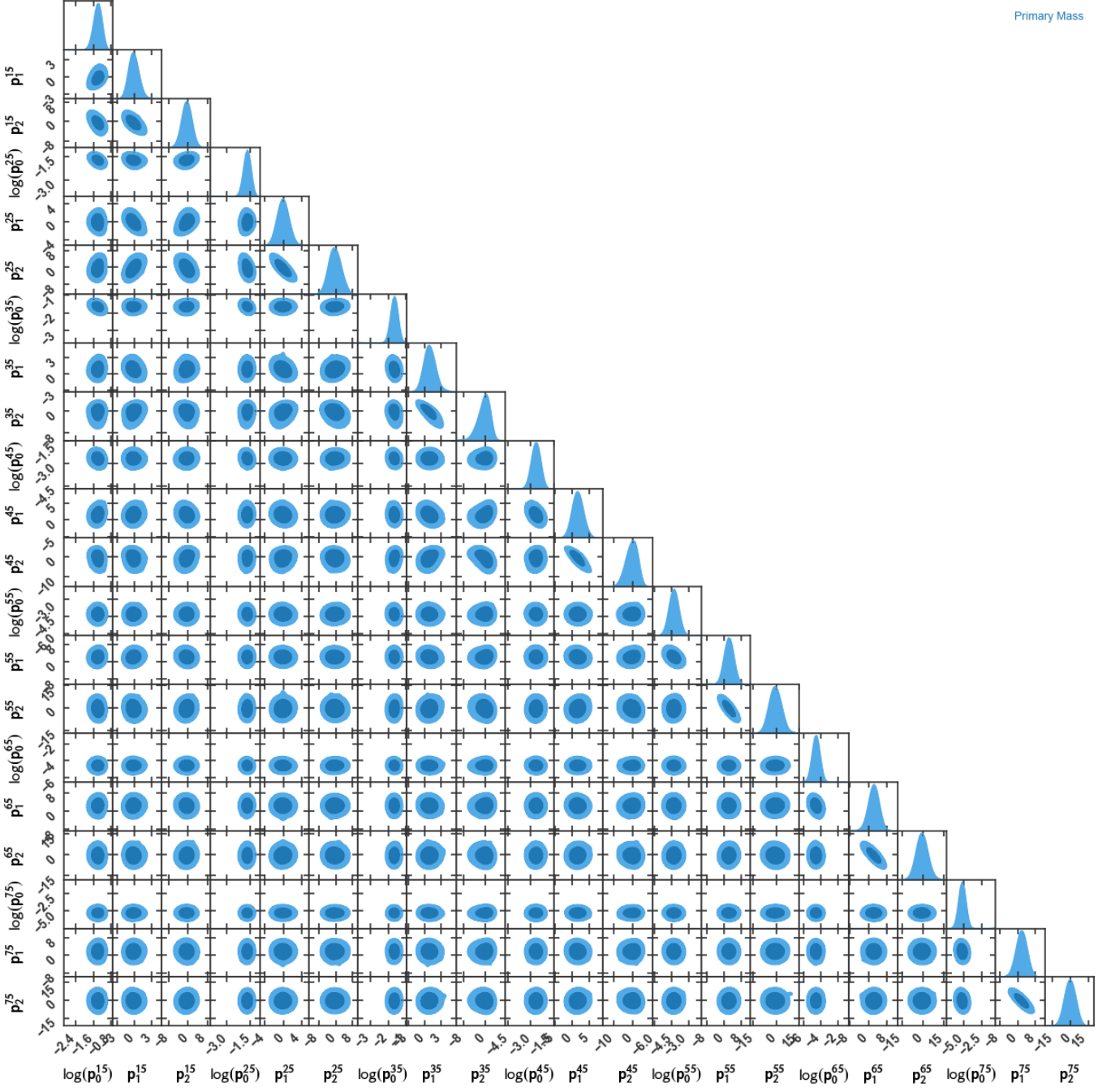


Figure 6. Corner plot showing the posterior distributions of the evolution coefficients for the primary black hole mass (m_1) using the coarse binning scheme ($\Delta M = 10M_\odot$). The parameters correspond to the Taylor expansion coefficients $\{p_0(m_k), p_1(m_k), p_2(m_k)\}$. The diagonal panels show the marginalized one-dimensional posterior distributions, while the off-diagonal panels show the joint posterior distributions with 1σ and 2σ credible regions. This configuration contains 21 parameters corresponding to the coefficients of the non-parametric reconstruction of the mass-redshift distribution.

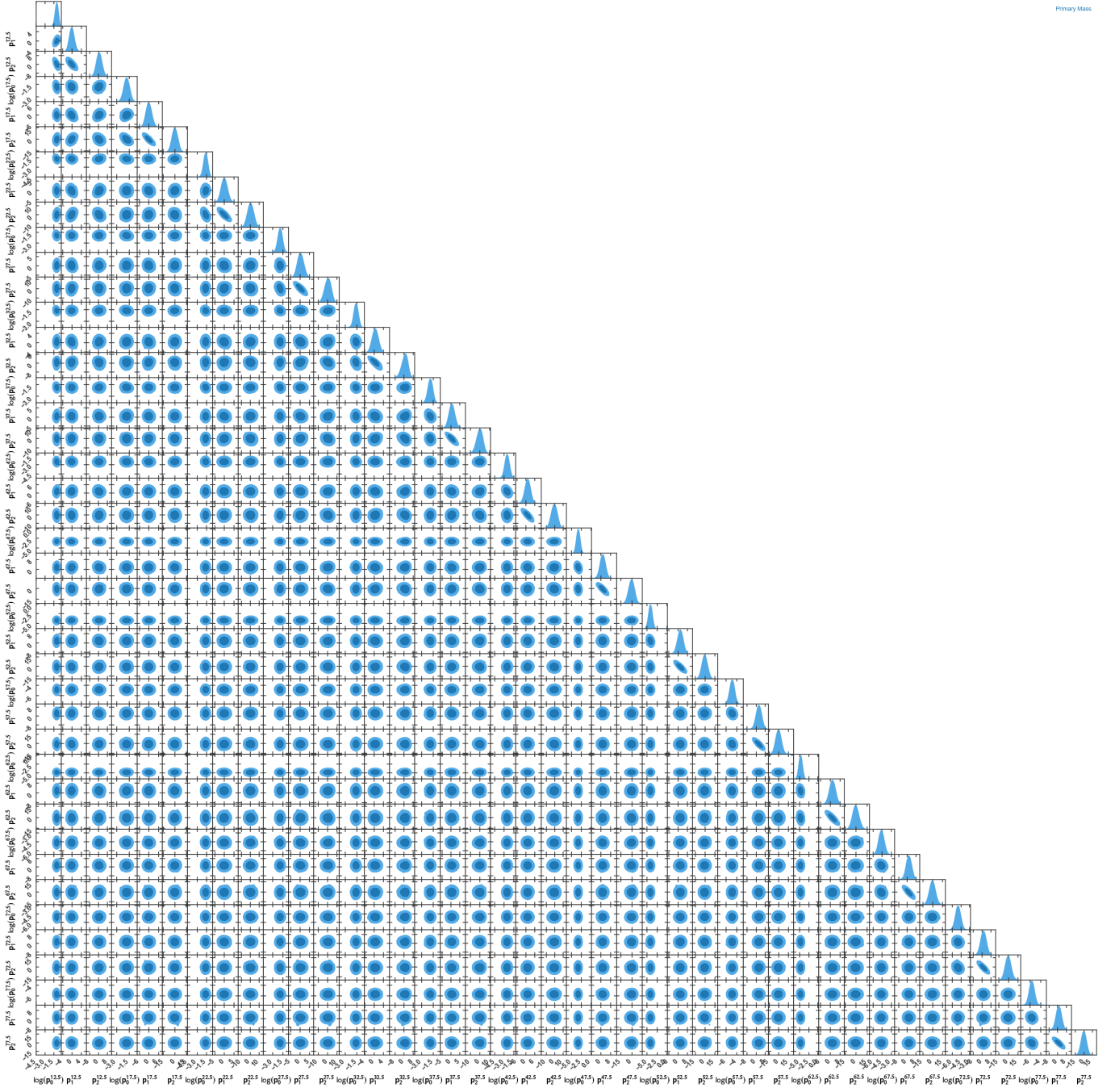


Figure 7. Corner plot showing the posterior distributions of the evolution coefficients for the primary black hole mass (m_1) using the finer mass binning scheme ($\Delta M = 5M_\odot$). The parameters again correspond to the coefficients $\{p_0(m_k), p_1(m_k), p_2(m_k)\}$. The increased number of bins leads to a higher-dimensional parameter space with 42 parameters in total.

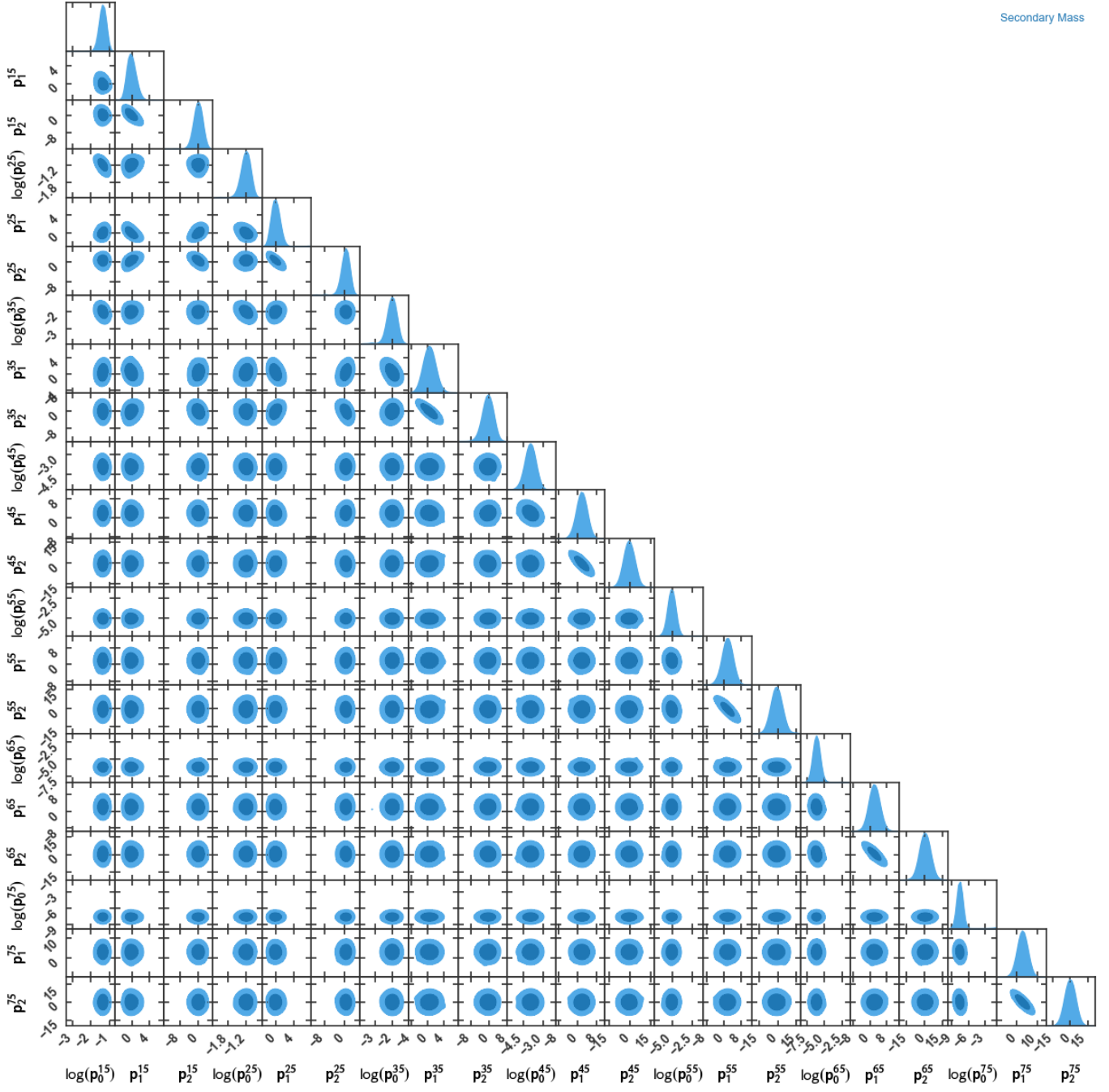


Figure 8. Corner plot showing the posterior distributions of the evolution coefficients for the secondary black hole mass (m_2) using the coarse binning scheme ($\Delta M = 10M_\odot$). The parameters correspond to the Taylor expansion coefficients $\{p_0(m_k), p_1(m_k), p_2(m_k)\}$ describing the redshift evolution of the secondary mass distribution. As in the primary mass analysis, the diagonal panels show marginalized one-dimensional posteriors while the off-diagonal panels show joint posterior distributions and parameter correlations.

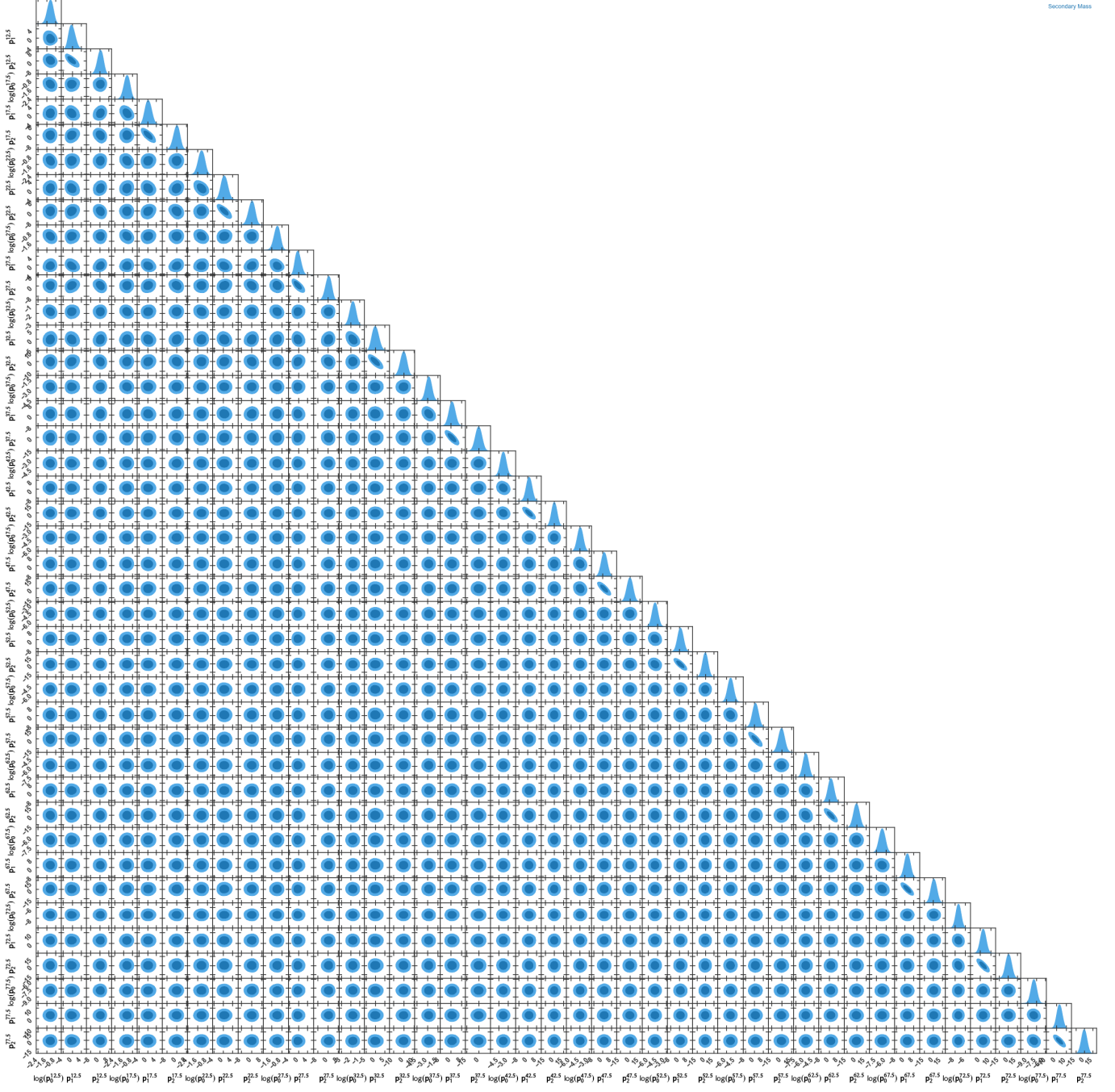


Figure 9. Corner plot showing the posterior distributions of the evolution coefficients for the secondary black hole mass (m_2) using the finer mass binning scheme ($\Delta M = 5M_\odot$). The larger number of mass bins leads to a higher-dimensional parameter space with 42 parameters. The corner plot illustrates the posterior constraints and correlations among all inferred coefficients in the hierarchical population model.

- Bouffanais, Y., Mapelli, M., Santoliquido, F., et al. 2021, *Mon. Not. Roy. Astron. Soc.*, 507, 5224, doi: [10.1093/mnras/stab2438](https://doi.org/10.1093/mnras/stab2438)
- Branchesi, M., et al. 2023, *JCAP*, 07, 068, doi: [10.1088/1475-7516/2023/07/068](https://doi.org/10.1088/1475-7516/2023/07/068)
- Callister, T. A., & Farr, W. M. 2024, *Phys. Rev. X*, 14, 021005, doi: [10.1103/PhysRevX.14.021005](https://doi.org/10.1103/PhysRevX.14.021005)
- Cheng, A. Q., Zevin, M., & Vitale, S. 2023, *Astrophys. J.*, 955, 127, doi: [10.3847/1538-4357/aced98](https://doi.org/10.3847/1538-4357/aced98)
- Costa, G., Ballone, A., Mapelli, M., & Bressan, A. 2022, *Mon. Not. Roy. Astron. Soc.*, 516, 1072, doi: [10.1093/mnras/stac2222](https://doi.org/10.1093/mnras/stac2222)
- Costa, G., Mapelli, M., Iorio, G., et al. 2023, *Mon. Not. Roy. Astron. Soc.*, 525, 2891, doi: [10.1093/mnras/stad2443](https://doi.org/10.1093/mnras/stad2443)
- Dominik, M., Belczynski, K., Fryer, C., et al. 2012, *Astrophys. J.*, 759, 52, doi: [10.1088/0004-637X/759/1/52](https://doi.org/10.1088/0004-637X/759/1/52)
- Dvorkin, I., Vangioni, E., Silk, J., Uzan, J.-P., & Olive, K. A. 2016, *Mon. Not. Roy. Astron. Soc.*, 461, 3877, doi: [10.1093/mnras/stw1477](https://doi.org/10.1093/mnras/stw1477)
- Edelman, B., Farr, B., & Doctor, Z. 2023, *Astrophys. J.*, 946, 16, doi: [10.3847/1538-4357/acb5ed](https://doi.org/10.3847/1538-4357/acb5ed)
- Essick, R. 2023, *Phys. Rev. D*, 108, 043011, doi: [10.1103/PhysRevD.108.043011](https://doi.org/10.1103/PhysRevD.108.043011)
- Essick, R., & Holz, D. E. 2024, *Phys. Rev. D*, 110, 103018, doi: [10.1103/PhysRevD.110.103018](https://doi.org/10.1103/PhysRevD.110.103018)
- Essick, R., et al. 2025. <https://arxiv.org/abs/2508.10638>
- Farah, A. M., Callister, T. A., Ezquiaga, J. M., Zevin, M., & Holz, D. E. 2025, *Astrophys. J.*, 978, 153, doi: [10.3847/1538-4357/ad9253](https://doi.org/10.3847/1538-4357/ad9253)
- Farmer, R., Renzo, M., de Mink, S., Fishbach, M., & Justham, S. 2020, *Astrophys. J. Lett.*, 902, L36, doi: [10.3847/2041-8213/abbadd](https://doi.org/10.3847/2041-8213/abbadd)
- Farmer, R., Renzo, M., de Mink, S. E., Marchant, P., & Justham, S. 2019, doi: [10.3847/1538-4357/ab518b](https://doi.org/10.3847/1538-4357/ab518b)
- Farrell, E. J., Groh, J. H., Hirschi, R., et al. 2021, *Mon. Not. Roy. Astron. Soc.*, 502, L40, doi: [10.1093/mnras/slaa196](https://doi.org/10.1093/mnras/slaa196)
- Fishbach, M., & Holz, D. E. 2017, *Astrophys. J. Lett.*, 851, L25, doi: [10.3847/2041-8213/aa9bf6](https://doi.org/10.3847/2041-8213/aa9bf6)
- Fishbach, M., Holz, D. E., & Farr, B. 2017, *Astrophys. J. Lett.*, 840, L24, doi: [10.3847/2041-8213/aa7045](https://doi.org/10.3847/2041-8213/aa7045)
- Fishbach, M., Doctor, Z., Callister, T., et al. 2021, *Astrophys. J.*, 912, 98, doi: [10.3847/1538-4357/abee11](https://doi.org/10.3847/1538-4357/abee11)
- Foreman-Mackey, D., Hogg, D. W., Lang, D., & Goodman, J. 2013, *Publications of the Astronomical Society of the Pacific*, 125, 306
- Franciolini, G., Baibhav, V., De Luca, V., et al. 2022, *Phys. Rev. D*, 105, 083526, doi: [10.1103/PhysRevD.105.083526](https://doi.org/10.1103/PhysRevD.105.083526)
- Gennari, V., Mastrogiovanni, S., Tamanini, N., Marsat, S., & Pierra, G. 2025, *Phys. Rev. D*, 111, 123046, doi: [10.1103/ftw9-7xd5](https://doi.org/10.1103/ftw9-7xd5)
- Gerosa, D., & Bellotti, M. 2024, *Class. Quant. Grav.*, 41, 125002, doi: [10.1088/1361-6382/ad4509](https://doi.org/10.1088/1361-6382/ad4509)
- Giacobbo, N., Mapelli, M., & Spera, M. 2018, *Mon. Not. Roy. Astron. Soc.*, 474, 2959, doi: [10.1093/mnras/stx2933](https://doi.org/10.1093/mnras/stx2933)
- Heinzel, J., Mould, M., Álvarez-López, S., & Vitale, S. 2025a, *Phys. Rev. D*, 111, 063043, doi: [10.1103/PhysRevD.111.063043](https://doi.org/10.1103/PhysRevD.111.063043)
- Heinzel, J., Mould, M., & Vitale, S. 2025b, *Phys. Rev. D*, 111, L061305, doi: [10.1103/PhysRevD.111.L061305](https://doi.org/10.1103/PhysRevD.111.L061305)
- Heinzel, J., Talbot, C., Ashton, G., & Vitale, S. 2023, *Mon. Not. Roy. Astron. Soc.*, 523, 5972, doi: [10.1093/mnras/stad1823](https://doi.org/10.1093/mnras/stad1823)
- Hendriks, D. D., van Son, L. A. C., Renzo, M., Izzard, R. G., & Farmer, R. 2023, *Mon. Not. Roy. Astron. Soc.*, 526, 4130, doi: [10.1093/mnras/stad2857](https://doi.org/10.1093/mnras/stad2857)
- Hunter, J. D. 2007, *Computing in science & engineering*, 9, 90
- Iorio, G., et al. 2022, *mnras*, doi: [10.1093/mnras/stad1630](https://doi.org/10.1093/mnras/stad1630)
- Jones, E., Oliphant, T., Peterson, P., et al. 2001–, *SciPy: Open source scientific tools for Python*. <http://www.scipy.org/>
- Karathanasis, C., Mukherjee, S., & Mastrogiovanni, S. 2023, *Mon. Not. Roy. Astron. Soc.*, 523, 4539, doi: [10.1093/mnras/stad1373](https://doi.org/10.1093/mnras/stad1373)
- Kimball, C., Talbot, C., L. Berry, C. P., et al. 2020, *Astrophys. J.*, 900, 177, doi: [10.3847/1538-4357/aba518](https://doi.org/10.3847/1538-4357/aba518)
- Kimball, C., et al. 2021, *Astrophys. J. Lett.*, 915, L35, doi: [10.3847/2041-8213/ac0aef](https://doi.org/10.3847/2041-8213/ac0aef)
- Lalleman, M., Turbang, K., Callister, T., & van Remortel, N. 2025, *Astron. Astrophys.*, 698, A85, doi: [10.1051/0004-6361/202553941](https://doi.org/10.1051/0004-6361/202553941)
- Leung, S.-C., Nomoto, K., & Blinnikov, S. 2019, *Astrophys. J.*, 887, 72, doi: [10.3847/1538-4357/ab4fe5](https://doi.org/10.3847/1538-4357/ab4fe5)
- LIGO-VIRGO-KAGRA Collaboration. 2025a. <https://arxiv.org/abs/2508.18083>
- . 2025b. <https://arxiv.org/abs/2508.18082>
- Loredo, T. J. 2004, *AIP Conf. Proc.*, 735, 195, doi: [10.1063/1.1835214](https://doi.org/10.1063/1.1835214)
- LVK Scientific Collaboration. 2021a, *GWTC-2.1: Deep Extended Catalog of Compact Binary Coalescences*, Zenodo, doi: [10.5281/zenodo.6513631](https://doi.org/10.5281/zenodo.6513631)
- . 2021b, *GWTC-3: Compact Binary Coalescences Observed by LIGO and Virgo*, Zenodo, doi: [10.5281/zenodo.5546663](https://doi.org/10.5281/zenodo.5546663)
- . 2025, *GWTC-4.0: Compact Binary Coalescences Observed by LIGO, Virgo, and KAGRA*, Zenodo, doi: [10.5281/zenodo.16053484](https://doi.org/10.5281/zenodo.16053484)

- Magaña Hernandez, I., & Palmese, A. 2025. <https://arxiv.org/abs/2508.19208>
- Mandel, I., Farr, W. M., & Gair, J. R. 2019, *Mon. Not. Roy. Astron. Soc.*, 486, 1086, doi: [10.1093/mnras/stz896](https://doi.org/10.1093/mnras/stz896)
- Mapelli, M. 2021, Formation Channels of Single and Binary Stellar-Mass Black Holes, doi: [10.1007/978-981-15-4702-7_16-1](https://doi.org/10.1007/978-981-15-4702-7_16-1)
- Messenger, C., & Veitch, J. 2013, *New J. Phys.*, 15, 053027, doi: [10.1088/1367-2630/15/5/053027](https://doi.org/10.1088/1367-2630/15/5/053027)
- Mukherjee, S. 2022, *Mon. Not. Roy. Astron. Soc.*, 515, 5495, doi: [10.1093/mnras/stac2152](https://doi.org/10.1093/mnras/stac2152)
- Ray, A., Magaña Hernandez, I., Mohite, S., Creighton, J., & Kapadia, S. 2023, *Astrophys. J.*, 957, 37, doi: [10.3847/1538-4357/acf452](https://doi.org/10.3847/1538-4357/acf452)
- Reitze, D., et al. 2019, *Bull. Am. Astron. Soc.*, 51, 035. <https://arxiv.org/abs/1907.04833>
- Riley, J., & Mandel, I. 2023, *Astrophys. J.*, 950, 80, doi: [10.3847/1538-4357/accf90](https://doi.org/10.3847/1538-4357/accf90)
- Rinaldi, S., Del Pozzo, W., Mapelli, M., Lorenzo-Medina, A., & Dent, T. 2024, *Astron. Astrophys.*, 684, A204, doi: [10.1051/0004-6361/202348161](https://doi.org/10.1051/0004-6361/202348161)
- Rinaldi, S., Liang, Y., Demasi, G., Mapelli, M., & Del Pozzo, W. 2025. <https://arxiv.org/abs/2506.05929>
- Robitaille, T. P., Tollerud, E. J., Greenfield, P., et al. 2013, *Astronomy & Astrophysics*, 558, A33
- Santoliquido, F., Mapelli, M., Iorio, G., et al. 2023, *Mon. Not. Roy. Astron. Soc.*, 524, 307, doi: [10.1093/mnras/stad1860](https://doi.org/10.1093/mnras/stad1860)
- Schiebelbein-Zwack, A., & Fishbach, M. 2024, *Astrophys. J.*, 970, 128, doi: [10.3847/1538-4357/ad5353](https://doi.org/10.3847/1538-4357/ad5353)
- Sicilia, A., Lapi, A., Boco, L., et al. 2022, *Astrophys. J.*, 924, 56, doi: [10.3847/1538-4357/ac34fb](https://doi.org/10.3847/1538-4357/ac34fb)
- Spera, M., & Mapelli, M. 2017, *Mon. Not. Roy. Astron. Soc.*, 470, 4739, doi: [10.1093/mnras/stx1576](https://doi.org/10.1093/mnras/stx1576)
- Talbot, C., Farah, A., Galaudage, S., Golomb, J., & Tong, H. 2025, *J. Open Source Softw.*, 10, 7753, doi: [10.21105/joss.07753](https://doi.org/10.21105/joss.07753)
- Talbot, C., Smith, R., Thrane, E., & Poole, G. B. 2019, *Phys. Rev. D*, 100, 043030, doi: [10.1103/PhysRevD.100.043030](https://doi.org/10.1103/PhysRevD.100.043030)
- Talbot, C., & Thrane, E. 2018, *Astrophys. J.*, 856, 173, doi: [10.3847/1538-4357/aab34c](https://doi.org/10.3847/1538-4357/aab34c)
- Tiwari, V. 2022, *Astrophys. J.*, 928, 155, doi: [10.3847/1538-4357/ac589a](https://doi.org/10.3847/1538-4357/ac589a)
- . 2025. <https://arxiv.org/abs/2507.15697>
- Tiwari, V., & Fairhurst, S. 2021, *Astrophys. J. Lett.*, 913, L19, doi: [10.3847/2041-8213/abf7e7](https://doi.org/10.3847/2041-8213/abf7e7)
- Tong, H., et al. 2025. <https://arxiv.org/abs/2509.04151>
- Van Der Walt, S., Colbert, S. C., & Varoquaux, G. 2011, *Computing in science & engineering*, 13, 22
- van Son, L. A. C., de Mink, S. E., Callister, T., et al. 2022, *Astrophys. J.*, 931, 17, doi: [10.3847/1538-4357/ac64a3](https://doi.org/10.3847/1538-4357/ac64a3)
- Wong, K. W. K., Breivik, K., Farr, W. M., & Luger, R. 2023, *ApJ*, 950, 181, doi: [10.3847/1538-4357/acc863](https://doi.org/10.3847/1538-4357/acc863)
- Wong, K. W. K., Contardo, G., & Ho, S. 2020, *Phys. Rev. D*, 101, 123005, doi: [10.1103/PhysRevD.101.123005](https://doi.org/10.1103/PhysRevD.101.123005)
- Wysocki, D., Lange, J., & O’Shaughnessy, R. 2019, *Phys. Rev. D*, 100, 043012, doi: [10.1103/PhysRevD.100.043012](https://doi.org/10.1103/PhysRevD.100.043012)
- Ye, C. S., & Fishbach, M. 2024, *Astrophys. J.*, 967, 62, doi: [10.3847/1538-4357/ad3ba8](https://doi.org/10.3847/1538-4357/ad3ba8)